CHAPTER 4: Optimisation for Sloshing

4.1 Introduction

This chapter covers all work done on the optimisation of sloshing, including the definition of the optimisation problem within the context of sloshing and how the software is set up to achieve automation of the optimisation process. Analysis for sloshing is done by the commercial CFD code Fluent v6.x [19], in the manner described in Chapter 3. The chapter includes results for all the single discipline optimisation for sloshing. The optimisation for sloshing includes both the use of 3D and 2D analyses of sloshing, as well as a comparison of different optimisation methodologies using less expensive 2D CFD analyses.

4.2 Definition of Objective Function

One of the major challenges in design optimisation for sloshing is the quantitative evaluation of an objective function. Implications of sloshing include the undesirable acoustical effect experienced in a vehicle fuel tank and issues related to dynamic feedback from oscillating liquids in aeroplanes or liquid transport containers. Ideally, one would like to remove any oscillatory motion, but also reduce the level of free-surface break up. Equation 4.1 below provides the formulation of a Total Deviation Value (TDV) that provides a single value for the level of sloshing that occurred over a period *t*. The value is essentially a numerical integration in time of the deviation of the free surface from its initial position of rest. As illustrated, the value is normalised by the number of computational or discretisation cells involved in the free surface, so that the number of cells encompassing the free surface do not affect the TDV.

$$TDV = \int_0^t \left(\sum_{xyz} \frac{\left| (surface\ height - initial\ level) \right|}{number\ of\ cells\ on\ free\ surface} \right) dt \qquad (4.1)$$

Figure 4.1 below provides an example of the deviation of the free surface versus time, where the TDV represents the area under the curve. The example represents a case without baffles, filled to 70% of capacity and exposed to a constant deceleration that corresponds to the tank decelerating from 60 to 0 km/h in 2 seconds. Figure 4.1 also provides images of the position of the free surface at various moments, for comparison with the corresponding calculated free-surface deviation at that time. The comparison clearly illustrates that the break-up of the free surface around 0.75 seconds causes an increase in the deviation value. Once the surface quietens, as it approaches its position of rest for the constant deceleration, the deviation levels off at the value corresponding to the resulting free-surface inclination. In a case with no baffles, the time to reach a state of equilibrium is quite long, due to the increase in free-surface area as the liquid oscillates. Figure 4.2 below illustrates 3 baffled cases and their corresponding deviations with time. Case 1 shows the worst case resulting from highly oscillatory motion, while case 2 shows an improvement, but free-surface break-up causes a peak near 0.7 seconds. Case 3 shows the best result with the lowest TDV. All three lines will converge eventually to the same value once the free surface has settled.

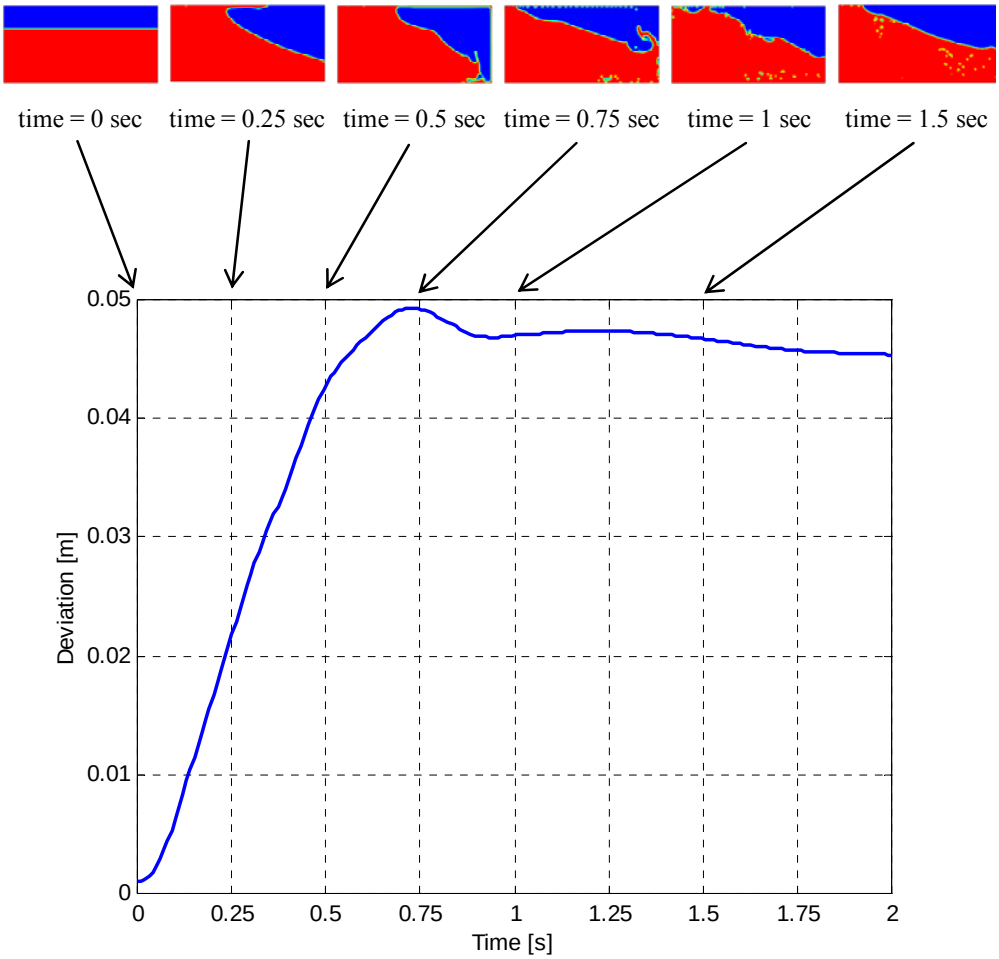

Figure 4.1: Example of free surface deviation versus time

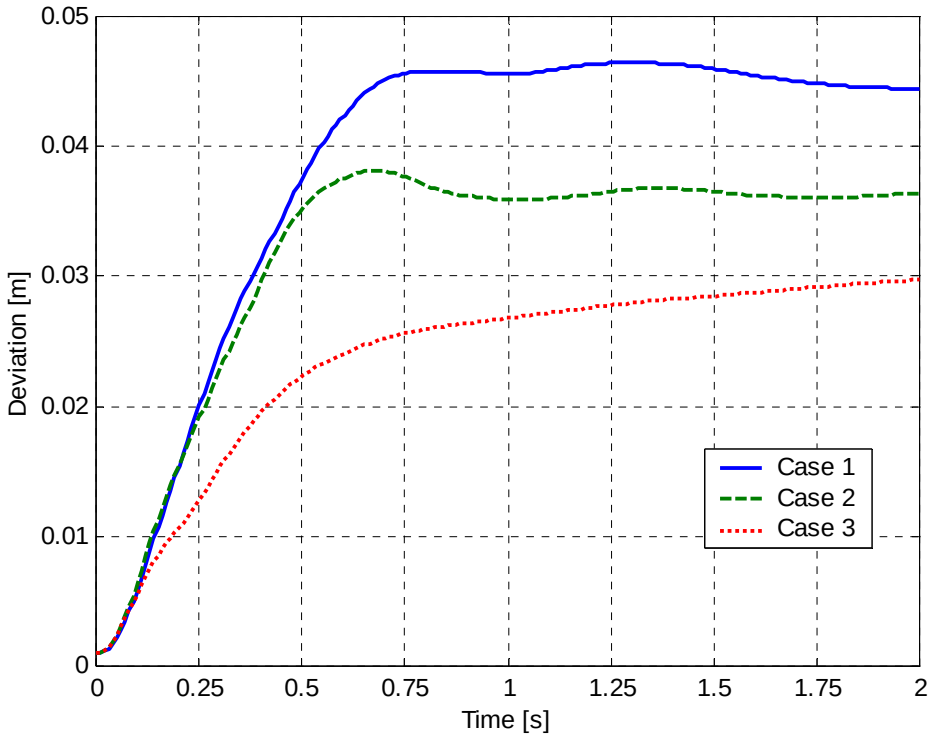

Figure 4.2: Free-surface deviation for 3 baffled cases

In summary, a low TDV results from a case where the free surface approaches its position of equilibrium (for the instantaneous acceleration) slowly, without any break up of the free surface, and without any oscillatory motion.

4.3 Optimisation Problem Setup

The setup of the optimisation problem describes the steps that are taken to ensure the partial or full automation of the optimisation procedure. This section describes the setup for all the optimisation for sloshing problems that are examined. All the cases examined in this section are performed according to the flow chart shown in Figure 2.12.

4.3.1 LS-OPT 3-D Sloshing Case Optimisation

The case examined here is a full 3-D representation of a partially-filled (50%) liquid container with zero-thickness baffles containing holes. Figure 4.3 below (Repeated from Figure 3.1) shows the form of the 3-D model of dimensions WxHxL = 400x400x500mm. The model is subject to a constant deceleration from 60 to 0 km/h in 5 seconds followed by zero deceleration for a further 2 seconds, i.e., the total transient time simulated is 7 seconds.

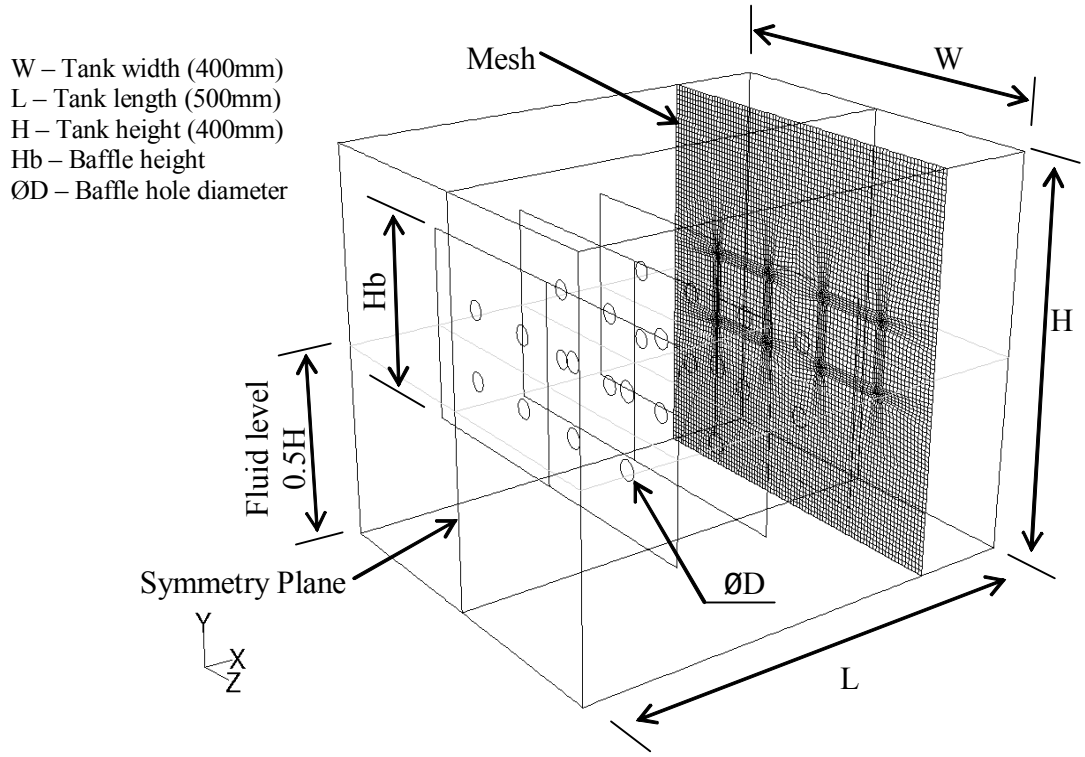

Figure 4.3: Geometry of 3-D sloshing case

This optimisation case involves the use of LS-OPT as the optimisation software, assuming linear successive response surfaces in one case and a Kriging meta-model in another (Appendix F provides the input command file used by LS-OPT). The user will initialise the design points to be analysed for each optimisation iteration. Pre-processing is done using Gambit with a journal file for the automated construction of the mesh (Appendix G provides the Gambit journal file used). A further journal file (Appendix H) is used in the automated setup of the model in Fluent, which models half of the geometry base on the symmetry plane shown in Figure 4.3. Post processing of the data generated by Fluent to extract the TDV is done by an executable file compiled from the C source code shown in Appendix I.

To complete a single Fluent analysis of a 3-D sloshing event takes approximately 48 hours on the available workstations (2GHz P4 Linux Workstations). Due to this long simulation time, only two design variables are considered in the optimisation. The optimisation problem is defined according to Equation 4.2 below:

$$\textit{Variables } \mathbf{x} = [x_1, x_2]^T \qquad (4.2)$$

x_1 = Hb = Baffle height

x_2 = ØD = Hole diameter

Objective:

Minimize $\{f(\mathbf{x}) = TDV\}$

Subject to:

Inequality constraints-

$$g_1(\mathbf{x}) = 10\text{mm} - \frac{x_1 - 4x_2}{5} < 0$$

$$g_2(\mathbf{x}) = \frac{x_1 - 2x_2}{3} - \frac{x_2}{2} - 8\text{mm} < 0$$

$$g_3(\mathbf{x}) = 400x_1 - 8\pi.x_2^2 - 95000\text{mm}^2 < 0$$

Side constraints-

$g_4(\mathbf{x})$: x_1 (Hb) (80;380)mm

$g_5(\mathbf{x})$: x_2 (ØD) (15;80)mm

Inequality constraints g_1 and g_2 are necessary to ensure that the model is geometrically feasible, e.g., that the holes do not get too large for the baffles, etc. The side constraints g_4 and g_5 represent the limits on the variables. Inequality constraint g_3 is put in place in anticipation of the design going toward large baffles with small holes. In this case one would like to make the problem more interesting by restricting the amount of material used (related to mass of baffles or cost of production). In this case arbitrarily chosen as 95 000mm^2. This case formed part of a study done in collaboration with R Dieterich in 2002 [53].

4.3.2 2-D Sloshing Cases Setup

Due to the expense of full 3-D CFD analyses, further analysis involved a 2-D simplification of the liquid container. A number of cases are examined, all involving one of two topological layouts that will be referred to as design 1 and design 2. Figure 4.4 and Figure 4.5 below show the geometries used in designs 1 and 2 respectively. All cases are subject to the same load derived from a constant deceleration from 60 to 0 km/h in 2 seconds (Appendix J provides a sample of the User-Defined Function (UDF) c-code used for a predefined acceleration). As in the 3-D case, pre-processing is done by Gambit with the use of a journal file (See sample 2-D Gambit journal in Appendix A) and the Fluent setup is done with its respective journal file (See sample 2-D Fluent journal in Appendix C). Appendix K provides the 2-D-adapted c source code for compiling the TDV extractor program.

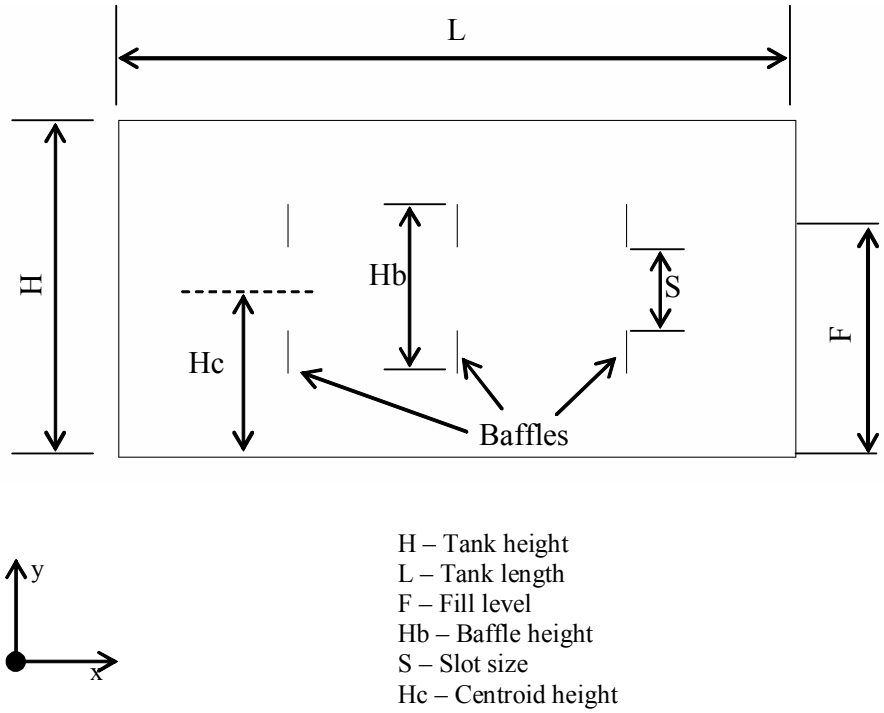

Figure 4.4: Geometry of 2-D container: Design-1

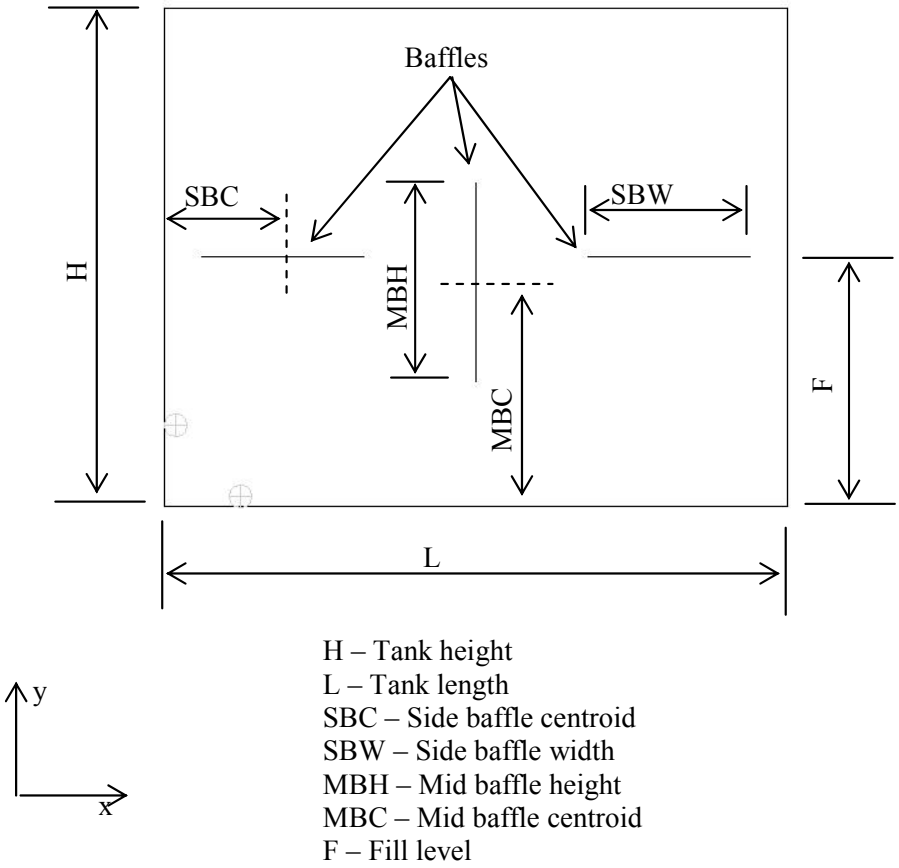

Figure 4.5: Geometry of 2-D container: Design-2

Table 4.1 below provides the general formulation of the 2-D optimisation cases considered. The abbreviations for the design variables are consistent with those used in Figure 4.4 and Figure 4.5 above. The sections that follow provide more in depth descriptions of the individual cases.

Table 4.1: Definition of optimisation cases (2D sloshing)

Case	Design type (HxL)	Fill	Optimisation method	Design variables	Constraints	Evaluations per iteration
1	**1** (200x400mm)	0.7H	Linear SRSM	$\mathbf{x}_{(1-3)}$= (Hc,Hb,S)	-Geometrical	7
2	**1** (200x400mm)	0.7H	Quadratic SRSM	$\mathbf{x}_{(1-3)}$= (Hc,Hb,S)	-Geometrical	16
3	**1** (200x400mm)	0.7H	Neural Network	$\mathbf{x}_{(1-3)}$= (Hc,Hb,S)	-Geometrical	129
4	**1** (200x400mm)	0.7H	Dynamic-Q	$\mathbf{x}_{(1-3)}$= (Hc,Hb,S)	-Geometrical	4
5	**2** (200x400mm)	0.7H	Quadratic SRSM	$\mathbf{x}_{(1-4)}$= (MBC,SBC, MBH,SBW)	-Geometrical	23
6	**2b** (400x500mm)	0.7H	Linear SRSM	$\mathbf{x}_{(1-4)}$= (MBC,SBC, MBH,SBW)	-Geometrical	8
7	**2** (200x400mm)	x_5*H (variable)	Quadratic SRSM	$\mathbf{x}_{(1-5)}$= (F,MBC,SBC, MBH,SBW)	-Geometrical -Fill level	32

4.3.2.1 Linear LS-OPT Design 1 (Case 1)

This case makes use of the Linear SRSM within the LS-OPT framework. Appendix L provides the LS-OPT command file for this case. The optimisation problem is defined as in Equation 4.3 below.

$$\textit{Variables } \mathbf{x} = [x_1, x_2, x_3]^T \tag{4.3}$$

x_1 = Hc = Baffle centroid height

x_2 = Hb = Baffle height

x_3 = S = Slot size

Objective:

Minimize {f(**x**) = TDV}

Subject to:

Inequality constraints-

$$g_1(\mathbf{x}) = -(190 - 0.5*x_2) + x_1 < 0$$
$$g_2(\mathbf{x}) = (10 + 0.5*x_2) - x_1 < 0$$
$$g_3(\mathbf{x}) = x_3 - 0.8*x_2 < 0$$

Side constraints-

$g_4(\mathbf{x})$: x_1 (Hc) (10;190)mm
$g_5(\mathbf{x})$: x_2 (Hb) (20;180)mm
$g_6(\mathbf{x})$: x_3 (S) (10;140)mm

Inequality constraints g_1 and g_2 ensure that the baffle does not come too close to either the roof or the floor of the container respectively. Inequality constraint g_3 ensures that the slot in the baffle does not become greater than 80% of the baffle height. The side constraints represent the limits of the variables. A linear SRSM is the simplest response surface method that makes use of 50% over-sampling provided by LS-OPT, in that it requires the least analyses per optimisation iteration.

4.3.2.2 Quadratic LS-OPT Design 1 (Case 2)

This case makes use of the quadratic successive response surface method within the LS-OPT framework. Appendix M provides the LS-OPT command file. The problem is defined exactly as in equation 4.3 above. Although the Quadratic SRSM requires more analyses per optimisation iteration, its performance should be evaluated against that of the Linear SRSM due to a possible bias or modelling error reduction.

4.3.2.3 Neural Network LS-OPT Design 1 (Case 3)

This case makes use of a single neural network meta-model within the LS-OPT framework. Appendix N provides the LS-OPT command file. In an attempt to construct a response surface representing a larger (more global) region of the 3-D design space, the user will provide all the points to be used for the single optimisation iteration, as well as their results. 129 analysis results are provided as obtained during the case 1, *4.3.2.2 quadratic LS-OPT design 1* optimisation analysis. The problem is defined exactly as in equation 4.3 above. The neural network result will provide an alternative answer to the Linear and Quadratic SRSMs from the perspective of a more global optimisation technique.

4.3.2.4 Dynamic-Q TDO Design 1 (Case 4)

This case makes use of the Dynamic-Q method within the TDO framework. Each analysis is initialised by the user. The use of TDO and Dynamic-Q is motivated by the desire to compare LS-OPT's meta-modelling methods with a gradient-based method as provided by TDO. The problem is defined exactly as in equation 4.3 of case 1, *4.3.2.1 Linear LS-OPT design 1* above.

4.3.2.5 Quadratic LS-OPT Design 2 (Case 5)

This case makes use of the quadratic successive response surface method within the LS-OPT framework. Appendix O provides the LS-OPT command file. The design 2 topology is motivated by the suggestion made during Rodriguez's studies of 1952 [1] that proposes locating flow dampers in the regions of highest velocity. The results for TDV should be compared with those obtained in the previous four optimisation analyses. The problem is defined as in Equation 4.4 below.

$$\textit{Variables } \mathbf{x} = [x_1, x_2, x_3, x_4]^T \tag{4.4}$$

x_1 = MBC = mid baffle centroid

x_2 = SBC = side baffle centroid

x_3 = MBH = mid baffle height

x_4 = SBW = side baffle width

Objective:

min {f(**x**) = TDV}

Subject to:

Inequality constraints-

$g_1(\mathbf{x}) = - x_2 + 0.5*x_4 + 10mm < 0$

$g_2(\mathbf{x}) = x_2 + 0.5*x_4 - 190mm < 0$

$g_3(\mathbf{x}) = x_1 + 0.5*x_3 - 190mm < 0$

$g_4(\mathbf{x}) = - x_1 + 0.5*x_3 + 10mm < 0$

Side constraints-

$g_5(\mathbf{x})$: x_1 (MBC) (15;185)mm

$g_6(\mathbf{x})$: x_2 (SBC) (15;185)mm

$g_7(\mathbf{x})$: x_3 (MBH) (10;180)mm

$g_8(\mathbf{x})$: x_4 (SBW) (10;180)mm

As before, all constraints are required for geometric feasibility.

4.3.2.6 Linear LS-OPT Design 2b (Case 6)

This case makes use of the linear successive response surface method within the LS-OPT framework. Appendix P provides the LS-OPT command file. The motivation for this analysis will only become clearer during the MDO analysis of chapter 6, where larger containers (corresponding to those used during validation phase 2) are analysed. The problem is defined much as in case 5, *section 4.3.2.5 Quadratic LS-*

OPT design 2 above except for the following constraints (Equation 4.5) that change due to the change in the dimensions of the container:

Inequality constraints- (4.5)

$$g_1(\mathbf{x}) = - x_2 + 0.5*x_4 + 10mm < 0$$
$$g_2(\mathbf{x}) = x_2 + 0.5*x_4 - 190mm < 0$$
$$g_3(\mathbf{x}) = x_1 + 0.5*x_3 - 340mm < 0$$
$$g_4(\mathbf{x}) = - x_1 + 0.5*x_3 + 40mm < 0$$

Side constraints-

$g_5(\mathbf{x})$: x_1 (MBC) (60;320)mm
$g_6(\mathbf{x})$: x_2 (SBC) (15;185)mm
$g_7(\mathbf{x})$: x_3 (MBH) (40;320)mm
$g_8(\mathbf{x})$: x_4 (SBW) (10;180)mm

4.3.2.7 Quadratic LS-OPT Saddle Design 2 (Case 7)

This case makes use of the quadratic successive response surface method within the LS-OPT framework. Appendix Q provides the LS-OPT command file. The motivation for this study is to analyse the effect of the fill level (H), previously assumed as 70% full, on the performance of the baffles. The setup will attempt to maximise TDV w.r.t. the fill level while minimising TDV w.r.t. the remaining variables, to try and establish the worst case. The problem is defined as follows in equation 4.6 below, with the definition making use of a saddle point analysis.

Variables $\mathbf{x} = [x_1, x_2, x_3, x_4]^T$ (4.6)

x_1 = F = fill level
x_2 = MBC = mid baffle centroid
x_3 = SBC = side baffle centroid
x_4 = MBH = mid baffle height

x_5 = SBW = side baffle width

Objective:

$$\min_{x_{i,i=1-4}} \left\{ \max_{x_5} (f(\mathbf{x}) = TDV) \right\}$$

Subject to:

Inequality constraints-

$g_1(\mathbf{x}) = - x_2 + 0.5*x_4 + 10\text{mm} < 0$

$g_2(\mathbf{x}) = x_2 + 0.5*x_4 - 190\text{mm} < 0$

$g_3(\mathbf{x}) = x_1 + 0.5*x_3 - 190\text{mm} < 0$

$g_4(\mathbf{x}) = - x_1 + 0.5*x_3 + 10\text{mm} < 0$

Side constraints-

$g_5(\mathbf{x})$: x_1 (MBC) (15;185)mm

$g_6(\mathbf{x})$: x_2 (SBC) (15;185)mm

$g_7(\mathbf{x})$: x_3 (MBH) (10;180)mm

$g_8(\mathbf{x})$: x_4 (SBW) (10;180)mm

$g_9(\mathbf{x})$: x_5 (F) (10;190)mm

As before, all constraints are required for geometric feasibility.

4.4 Optimisation Results

The following section provides the results of the optimisation analyses described in section 4.3 above. Results will include the improvement of the design w.r.t. its starting value as well as the progression of all the variables and objective during the optimisation process. The various optimisation methods will be compared with each other on the basis of their results and how economically they are attained.

4.4.1 LS-OPT 3-D Sloshing Case Optimisation

As stated in section 4.3.1 this case formed part of a study conducted in collaboration with R Dieterich in 2002 [52]. As stated before, this study involved a Linear SRSM approach and a Kriging meta-model approach. Table 4.2 below gives the final results for both approaches. Figure 4.6 below illustrates the progress of the Linear RSM optimisation run. The figure does show that the solution converged after one iteration, however the result of the Kriging optimisation method suggests that the local optimum lies elsewhere. This confirms that further linear SRSM optimisation iterations are necessary to locate the true local optimum.

Table 4.2: 3-D sloshing LS-OPT optimisation results

	Starting value	Converged linear SRSM result	CFD computed	Converged Kriging model result	CFD computed
Hb (x_1) [mm]	300	80	80	120.9	120.9
ØD (x_2) [mm]	40	15	15	27.7	27.7
f*10^4 **[mm^2.s]**	27.10	20.03	21.31	19.02	**19.87**

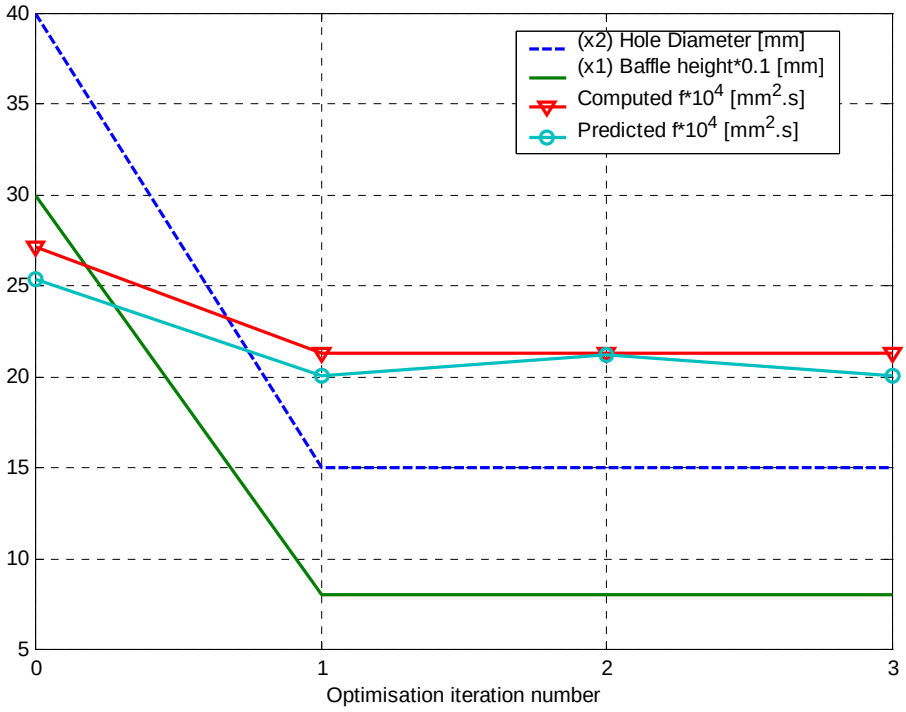

Figure 4.6: Linear SRSM optimisation history (3D sloshing)

The Kriging model is constructed from the points listed in Table 4.3 below, some of which come from the Linear RSM optimisation run. The resulting Kriging surface can be seen in Figure 4.7 below. Since this is an optimisation case with only 2 variables, it is quite simple to visualise a response surface like the one created by the Kriging interpolation method. The advantage of this method is that one can get a more global perspective on the response in question. As one can see an improved optimum existed slightly further along the active second inequality constraint (gap between hole and baffle edge). (Linear optimum shown for comparison on Figure 4.7)

Table 4.3: Points used for Kriging meta-model

Hb [mm]	80	139.15	147.5	170	170	187.7	200	200
ØD [mm]	15	15	35.29	15	35	15	15	20
***f*10^4* [mm².s]**	21.31	23.15	19.68	23.99	20.88	24.53	24.80	23.63
Hb [mm]	230	236.6	300	339.3	339.4	380	380	
ØD [mm]	59.7	15	40	15	64	15	80	
***f*10^4* [mm².s]**	24.66	25.54	27.13	25.26	31.07	20.47	34.17	

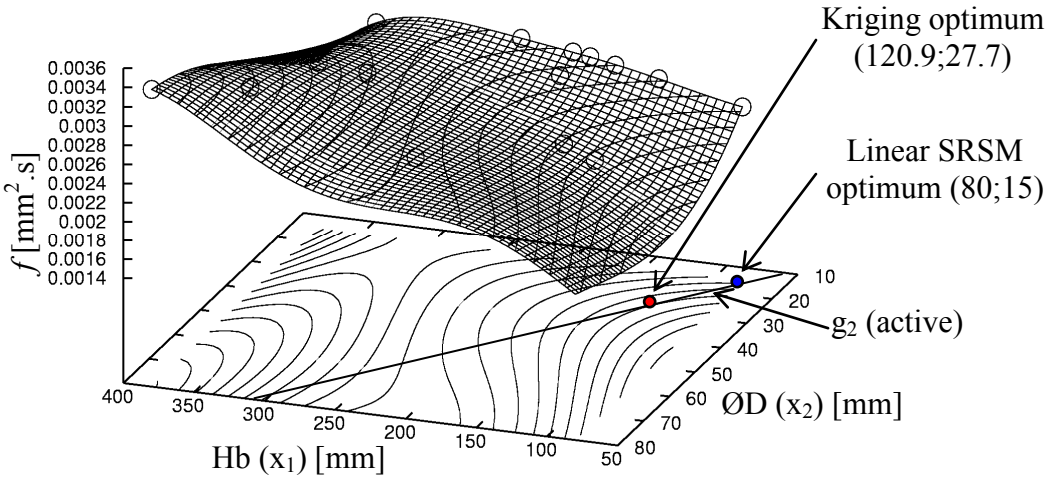

Figure 4.7: Kriging surface of 3-D sloshing case (with permission J Haarhoff)

The behaviour of the objective is clearly non-linear in the region of the optimum, which would explain the inability of the Linear RSM to locate it early in the optimisation process. However, it should be said that the Linear RSM would most likely have eventually found the global optimum once the design sub-region had been sufficiently reduced. This case makes a strong argument for the use of perhaps a

Quadratic RSM or a global meta-model like Kriging which is able to handle nonlinearities and thus reduce bias error.

Upon inspecting the objective response in Figure 4.7 one can make some conclusions about the effectiveness of baffles. Large baffles with small holes perform relatively poorly due to an effect best described as compartmentalisation. In effect the liquid container is merely subdivided into a number of smaller containers that have very little flow damping ability. The idea is to reduce the energy in the liquid, and since the highest velocities are seen near the free surface, this is where the flow damping should be done. This idea is confirmed with the result of the optimisation being small baffles with medium size holes. The small baffles allow flow past them so as not to compartmentalise the container, but still induces flow losses as the liquid passes over or under the baffle. The medium size holes continue this principle since the smallest holes will most likely not allow much flow through them and as a result not induce much damping. The larger holes will in turn allow too much liquid through an also not provide as much damping.

As a final comment on this optimisation case, the Linear RSM method required 15 function evaluations to attain a 21.3% improvement in the objective (from an arbitrary starting design), while the Kriging method attained a 26.7% improvement with the same number of function evaluations. It would also appear that the Kriging optimum is near the local minimum for this case, but would require more function evaluation (specifically near the area of the local optimum) to provide an accurate representation of the response.

4.4.2 2-D Sloshing Optimisation Results

4.4.2.1 Linear LS-OPT Design 1 (Case 1)

Table 4.4 below shows the final results for the Linear RSM optimisation of a design 1 2-D container. The result for TDV represents an improvement of 37.8% and required 50 function evaluations in 7 optimisation iterations. Figure 4.8 below shows the progress of the optimisation versus optimisation iteration number. Although this plot

represents the results obtained from 70 function evaluations (10 iterations), the optimum was found after the 7th iteration. Only one inequality constraint is active at the optimum and that is $g_2(\mathbf{x})$, which prevents the baffle from moving too low. It is interesting to note that the side constraint for the hole size is also active (Minimum slot size S (x_3) = 10mm). This indicates that the 2-D assumption applied to the model, resulting in a slot instead of a hole, provides very little flow damping. Furthermore, the design trend suggests a medium size baffle, the upper half of which tries to intercept the high velocities of the free surface. In effect, the lower half of the baffle is probably somewhat inactive. For the purposes of later comparison it should also be stated that the total length of baffle used (for all the baffles) is 373.8mm.

Table 4.4: Final results for Linear RSM design 1

	Starting value	Converged linear RSM result
Hc (x_1) [mm]	100	77.28
Hb (x_2) [mm]	100	134.6
S (x_3) [mm]	50	10
TDV (f*10^4) **[m.s]**	36.46	**22.66**

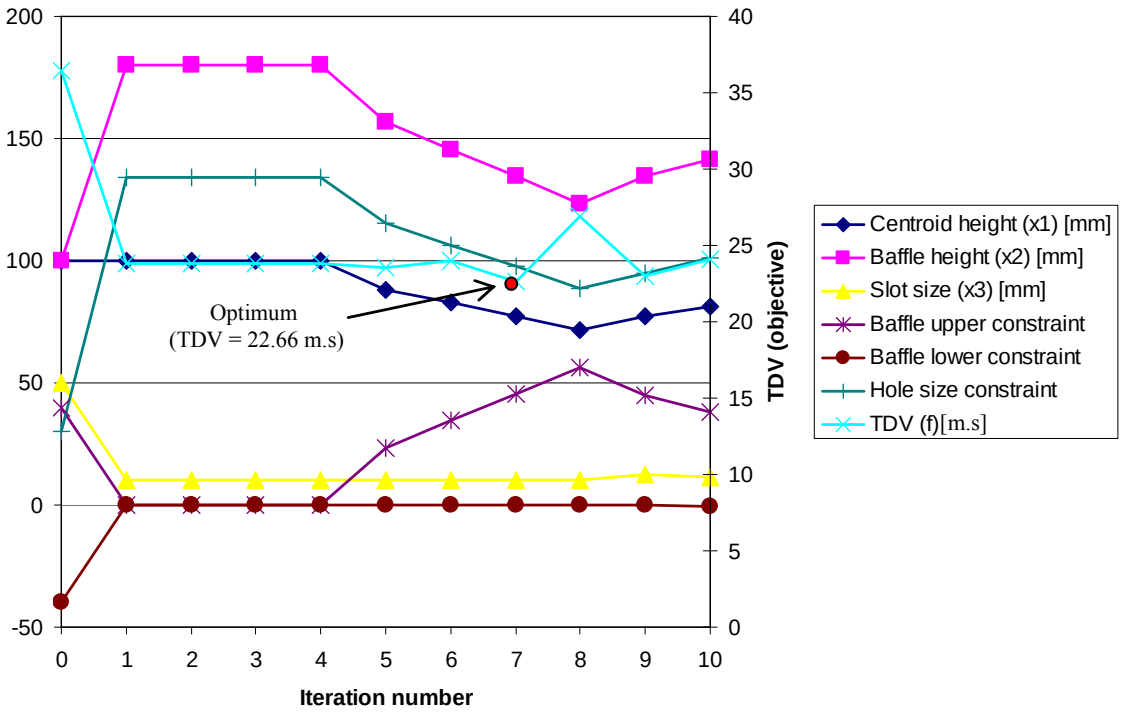

Figure 4.8: Optimisation history for Linear RSM design 1

When examining the 1st four optimisation iterations in Figure 4.8 above, it is clear that the non-linear behaviour of the problem only becomes evident to the optimisation algorithm once the design subspace has been sufficiently reduced in size. Figure 4.9 below gives a good illustration of the domain reduction for the variable x_1 (Baffle centroid). The result does however suggest a significant bias error due to the linear response assumption when applied to the initial large domain.

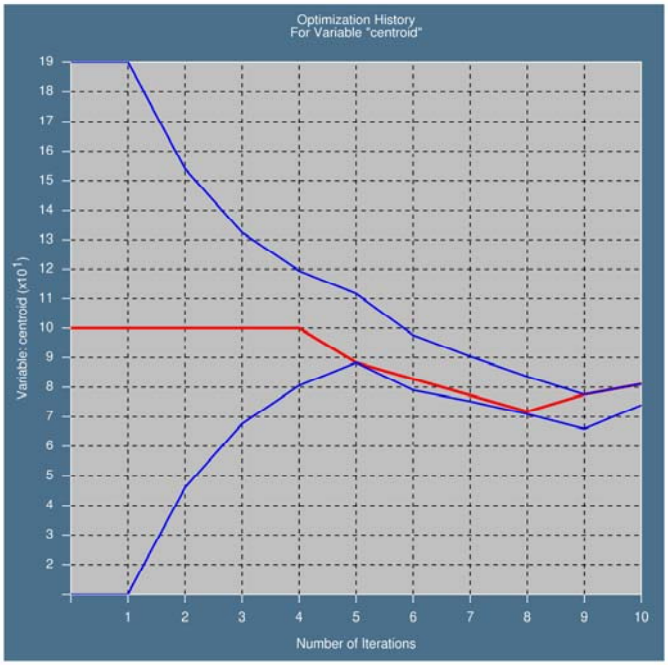

Figure 4.9: Design domain/subspace reduction for Baffle centroid (x_1)

4.4.2.2 Quadratic LS-OPT Design 1 (Case 2)

Table 4.5 below shows the final results for the Quadratic RSM optimisation of a design 1 2-D container. The result for TDV represents an improvement of 36.2% and required 128 function evaluations in 8 optimisation iterations for convergence. Figure 4.10 below shows the progress of the optimisation versus optimisation iteration number. The results are very similar to those obtained in the Linear RSM optimisation, although the Quadratic RSM run required 45.3% more function evaluations. What is clear from Figure 4.10 is that the Quadratic response assumption exhibited far less bias error side effects. The variables start converging toward the optimum almost immediately but approached it more slowly than the Linear RSM optimisation run.

Table 4.5: Final results for Quadratic RSM design 1

	Starting value	Converged linear RSM result
Hc (x_1) [mm]	100	76.68
Hb (x_2) [mm]	100	133.6
S (x_3) [mm]	50	10
***TDV (f*10^4)* [m.s]**	36.46	**23.26**

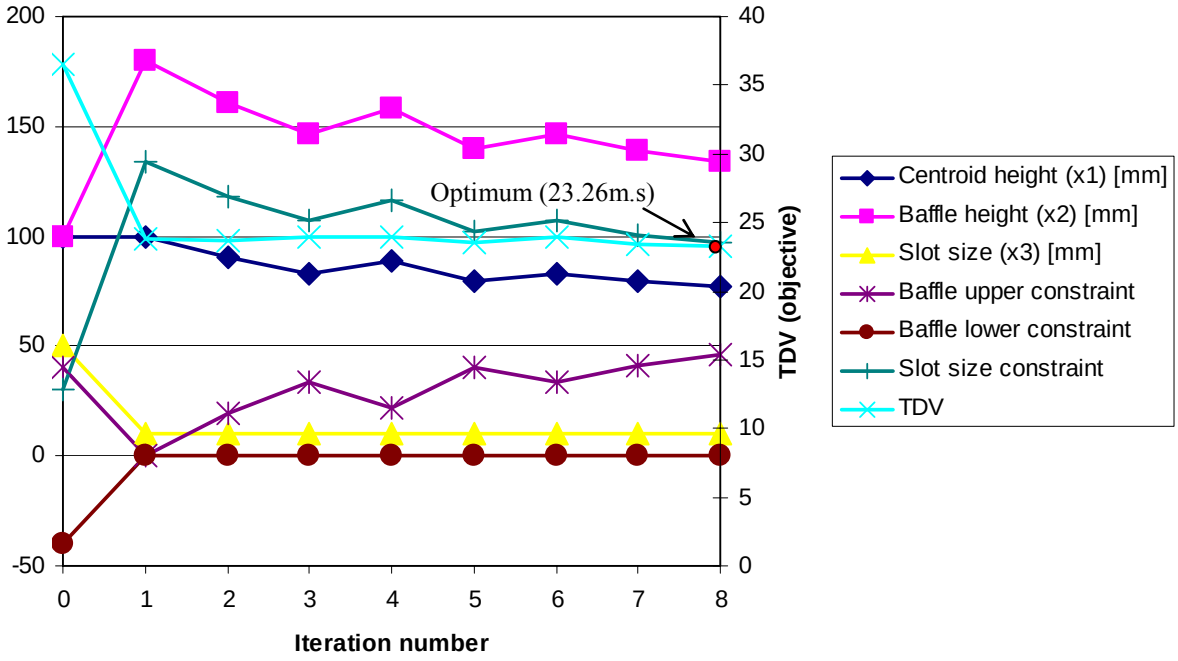

Figure 4.10: Optimisation history for Quadratic RSM design 1

An interesting analysis of the results is provided when examining a trade off between responses or variables. In particular, a trade-off study was performed between the objective TDV and the length of baffle used. The latter could be equated to the cost of the materials used. Figure 4.11 below illustrates the trade-off curves generated for each optimisation iteration. The trade-off curve (approximated Pareto-optimal front)

is generated by linking a specified number of points that are the predicted optimum results for the objective (TDV) for the response value in question (baffle length in this case) from the data received during a particular iteration. Some interesting observation can be made about trade-off curves. The curve provides the observer with the opportunity to decide what level of performance is required and how much material he/she is willing to use. From this perspective, the 1st three curves provide the most meaningful data. Due to the domain subspace reduction, the curves that follow don't provide much of a global perspective and are only valid in the immediate region of the subdomain optimum. Considering the trade-off curve illustrated for iteration 2, to achieve a TDV = 36 m.s, then 125 mm of baffle is required. If however the TDV needs to be reduced to TDV = 24 m.s, then 500 mm of baffle is required.

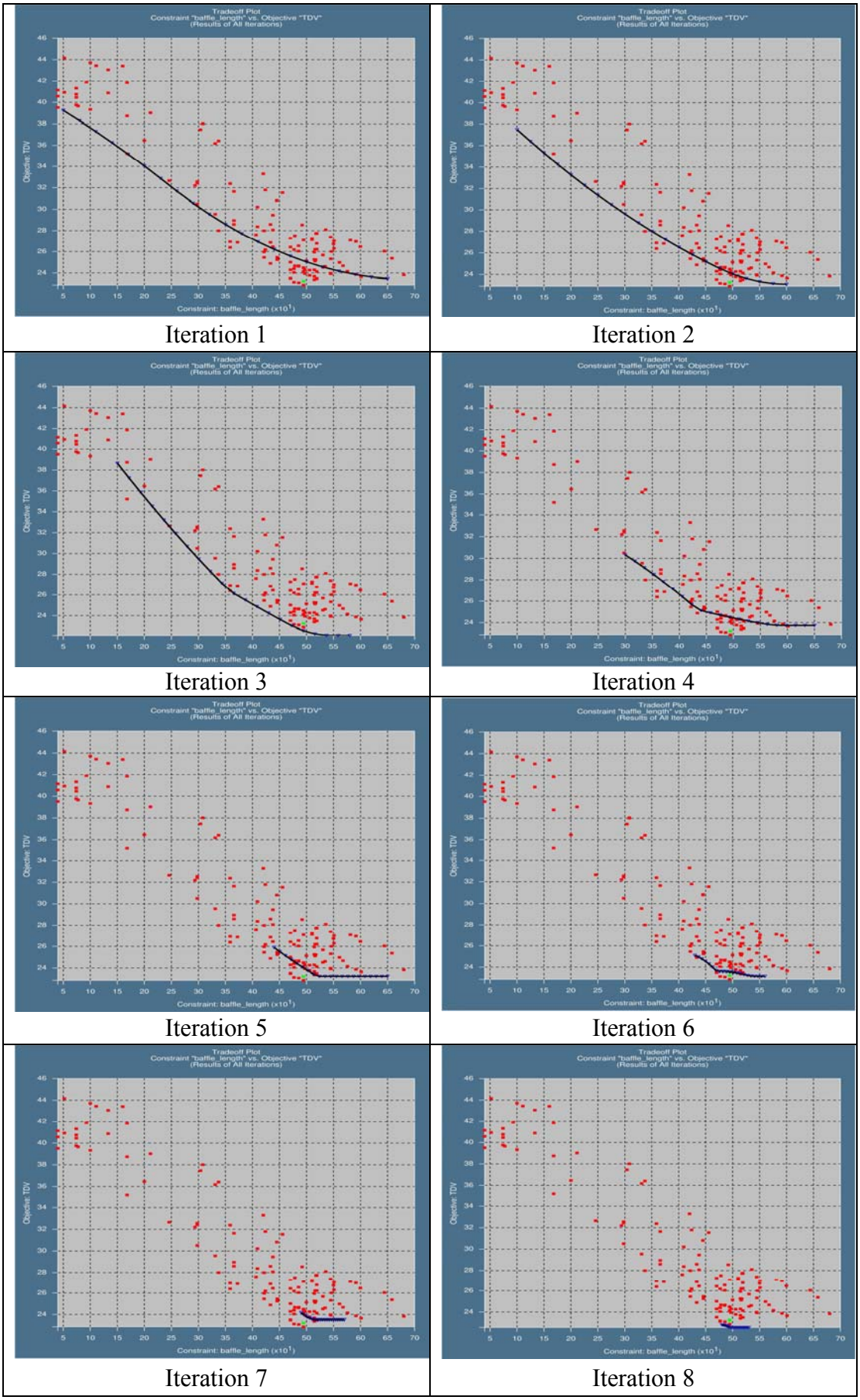

Figure 4.11: Trade-off progress for Quadratic RSM design 1

The final trade-off curve (iteration 8) gives more accurate data in terms of the absolute optimum, but when considering the potential use of trade-off curves is perhaps unnecessary to consider. In fact, if your objective is to do a trade-off study, it is only necessary to complete two or three optimisation iterations.

However since this is an optimisation study, the points of interest include that the maximum length of baffle available does not provide the absolute optimum.

4.4.2.3 Neural Network LS-OPT Design 1 (Case 3)

Table 4.6 below shows the final results for the Neural Network optimisation of a design 1 2-D container. The result for TDV represents an improvement of 27.6% and utilised 128 function evaluations in a single optimisation iteration. The total length of baffle used is 349.5mm.

Table 4.6: Final results for Neural Network Design 1

	Starting value	Converged linear RSM result
Hc (x_1) [mm]	100	73.24
Hb (x_2) [mm]	100	126.5
S (x_3) [mm]	50	10
***TDV (f*10^4)* [m.s]**	36.46	**26.41**

4.4.2.4 Dynamic-Q TDO Design 1 (Case 4)

Table 4.7 below shows the final results for the TDO Dynamic-Q optimisation of a design 1 2-D container. The result for TDV represents an improvement of 36.4% and utilised 40 function evaluations in 10 optimisation iterations. Figure 4.12 below shows the progress of the optimisation versus optimisation iteration number. Due to the differing nature of the Dynamic-Q method (i.e., spherically quadratic subproblem with move limits), the progress of the algorithm is clearly different in nature. The results are consistent with those seen previously with the methods available in LS-OPT. The total length of baffle used is 378mm.

Table 4.7: Final results for Dynamic-Q Design 1

	Starting value	Converged linear RSM result
Hc (x_1) [mm]	100	78
Hb (x_2) [mm]	100	136.0
S (x_3) [mm]	50	10
TDV (f*10^4) **[m.s]**	36.46	**23.18**[*]

[*] The results for TDV during the optimisation process where calculated using Fluent v5, but were confirmed with Fluent v6, with the results from the former being consistently lower (22.88 optimum versus 23.18).

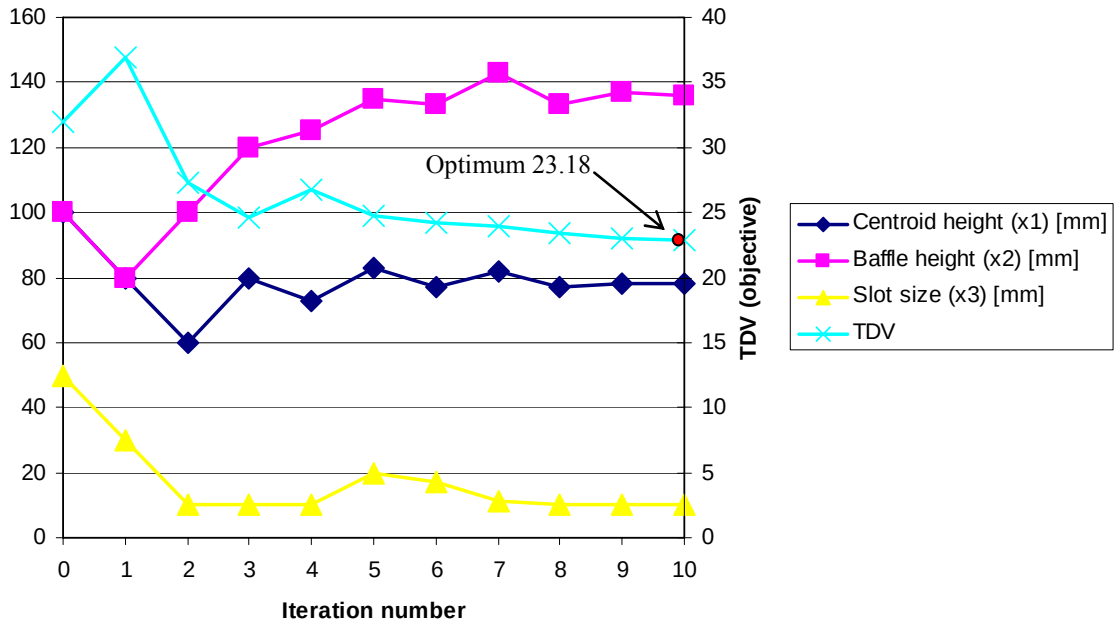

Figure 4.12: Optimisation history for Dynamic-Q design 1

Although the method requires significantly less function evaluations, it should be mentioned that a significant level of user intervention was necessary. Since the method is a gradient-based method it is susceptible to becoming unstable when noise enters the gradient calculations. A remedy to this instability is to impose move limits for the variables to prevent the divergence of the algorithm and to prevent it from overshooting local minima. The choice of the size of these move limits is not typically intuitive beforehand. A small move limit may also result in a very long convergence time. A further value that needs specification is the perturbation size for the finite difference gradient calculation. The incorrect choice of this value may result in the algorithm being adversely affected by the noise exhibited in most engineering problems. Ultimately, response surface methods illustrated significantly more robustness in the problem of optimisation for sloshing.

4.4.2.5 Quadratic LS-OPT Design 2 (Case 5)

Table 4.8 below shows the final results for the Quadratic RSM optimisation of a design 2 2-D container. The result for TDV represents an improvement of 16.7% and utilised 184 function evaluations in 8 optimisation iterations. Figure 4.13 below

shows the progress of the optimisation versus optimisation iteration number. The total length of baffle used is 418.8mm. The only active inequality constraint for this design is $g_4(\mathbf{x})$, which prevents the middle baffle from moving too low.

Table 4.8: Final results for Quadratic RSM design 2

	Starting value	Converged linear RSM result
MBC (x_1) [mm]	100	80.8
SBC (x_2) [mm]	100	79.29
MBH (x_3) [mm]	100	141.6
SBW (x_4) [mm]	100	138.6
***TDV ($f*10^4$)* [m.s]**	27.03	**22.52**

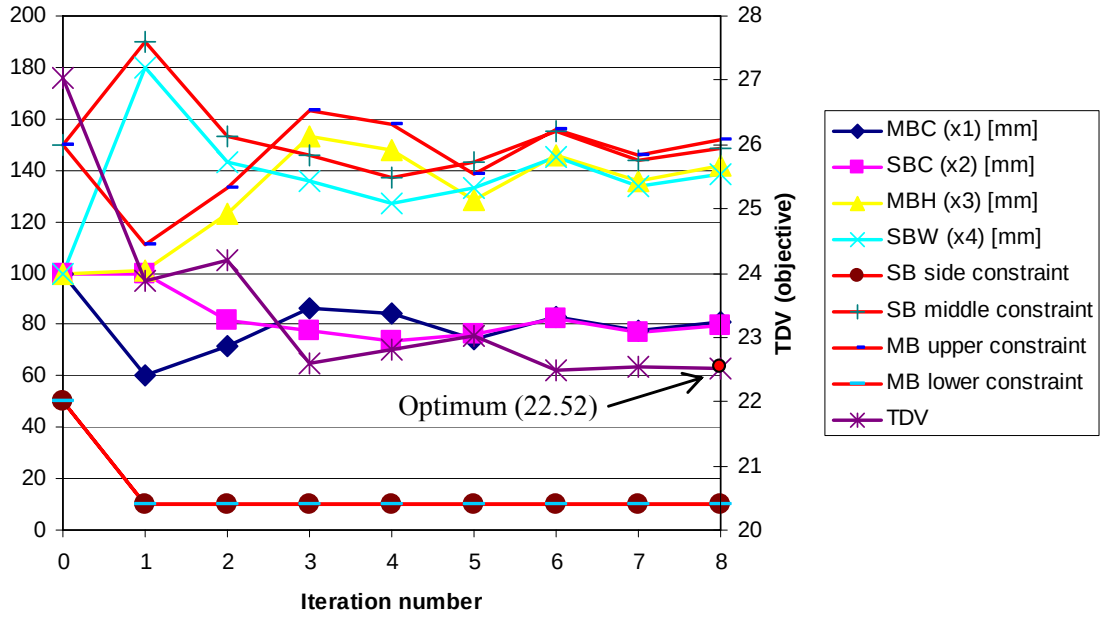

Figure 4.13: Optimisation history for Quadratic RSM design 2

The final result does provide a slight improvement for the optimum when compared to the design 1 container. However, the small improvement in TDV relative to the starting value does suggest a better overall design (one vertical and two horizontal baffles versus vertical slotted baffles).

4.4.2.6 Linear LS-OPT Design 2b (Case 6)

Table 4.9 below shows the final results for the Linear RSM optimisation of a design 2b 2-D container. The result for TDV represents an improvement of 40.3% and utilised 81 function evaluations in 10 optimisation iterations. Figure 4.14 below shows the progress of the optimisation versus optimisation iteration number. The total length of baffle used is 519mm. These results will be considered in conjunction with results in Chapter 5, when examining MDO of the liquid container in Chapter 6. The reason for repeating the 2D sloshing analysis for this case is to obtain a new TDV value for a higher container (400mm as apposed to 200mm). TDV is influenced by the height of the container since more space above the initial free-surface level will allow more deviation of the active free surface during the sloshing event from its initial location. Appendix R shows comparative frames, during the sloshing analysis, for the base case and the final design.

Table 4.9: Final results for Linear RSM design 2b

	Starting value	Converged linear RSM result
MBC (x_2) [mm]	100	162
SBC (x_3) [mm]	100	78
MBH (x_4) [mm]	100	244
SBW (x_5) [mm]	100	136
TDV ***($f*10^4$)*** **[m.s]**	49.17	**29.37**

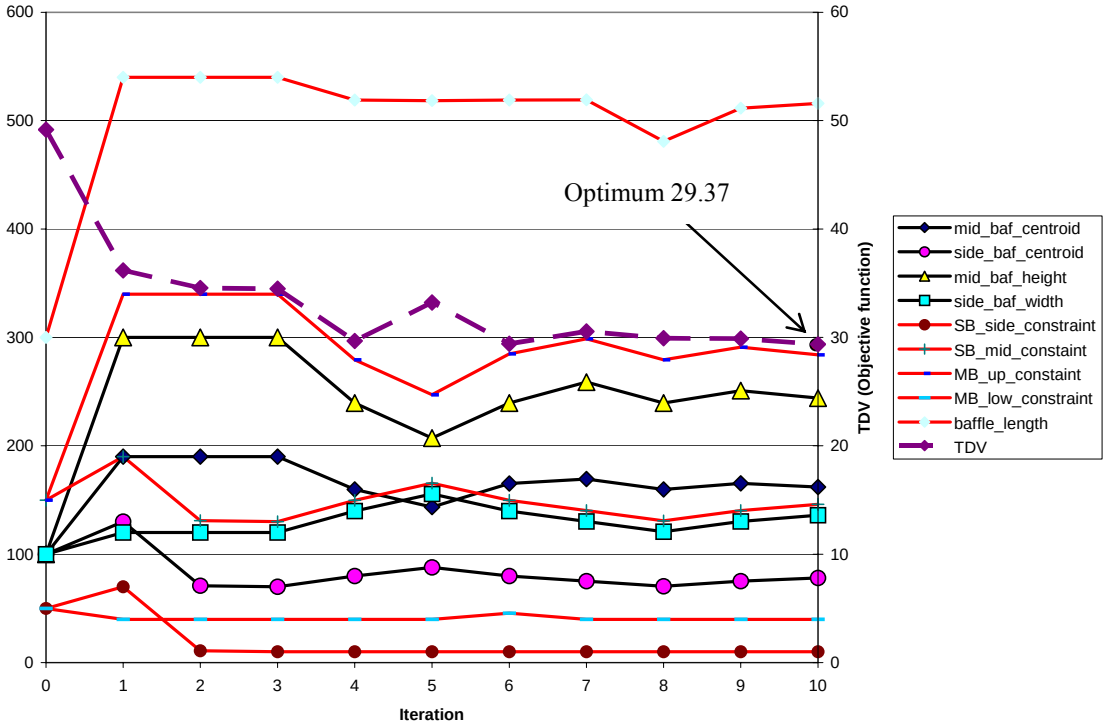

Figure 4.14: Optimisation history for Linear RSM Design 2b

4.4.2.7 Quadratic LS-OPT Saddle Point Design 2 (Case 7)

Table 4.10 below shows the final results for the Quadratic RSM saddle-point optimisation of a design 2 2-D container. The result for TDV represents an improvement of 27.8% and utilised 257 function evaluations in 8 optimisation iterations. Figure 4.15 below shows the progress of the optimisation versus optimisation iteration number. The total length of baffle used is 442.8mm. These optimisation analysis results provide some level of confidence in the final design variable values attained, since the result for TDV represent the worst TDV that would occur for the set of variable values that the optimisation algorithm converged to.

Table 4.10: Final results for Quadratic RSM saddle point Design 2

	Starting value	final linear RSM result
F (x_1) [m]	0.1 (50% full)	0.153 (77% full)
MBC (x_2) [mm]	100	83.7
SBC (x_3) [mm]	100	86
MBH (x_4) [mm]	100	139
SBW (x_5) [mm]	100	151.9
***TDV ($f*10^4$)* [m.s]**	33.56	**24.23**

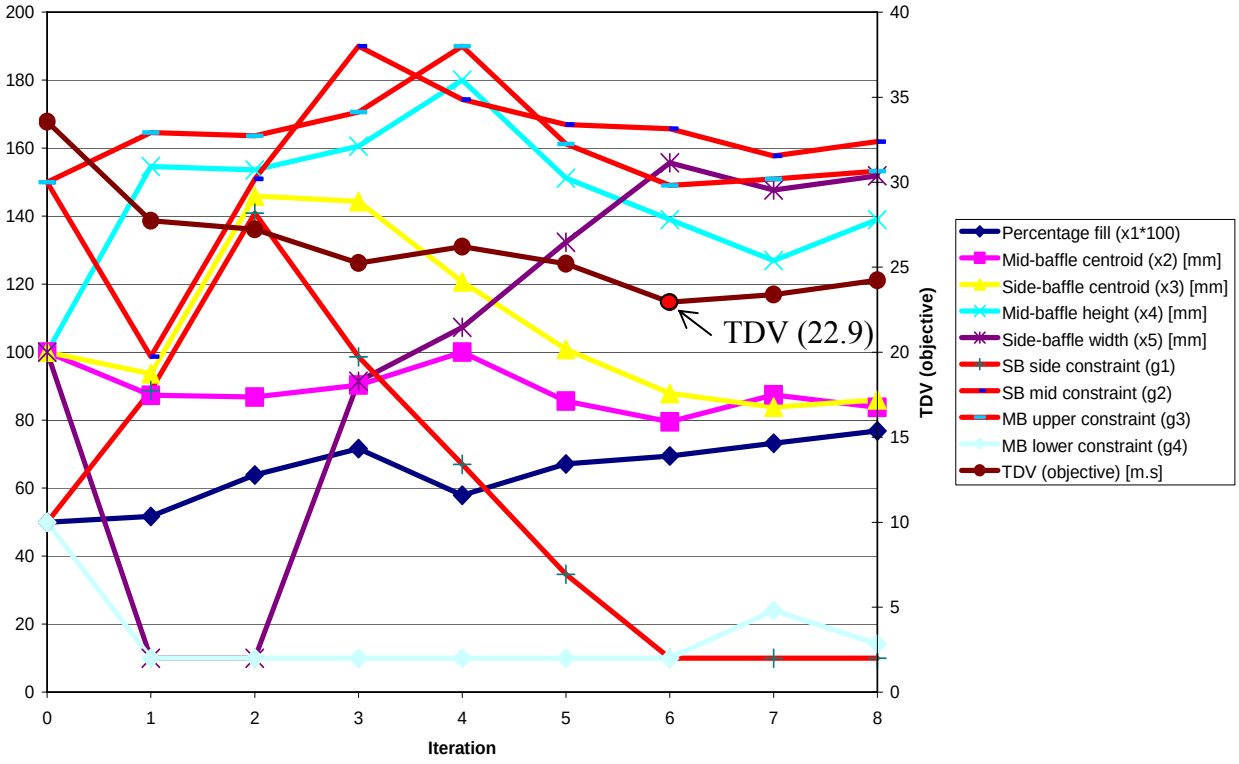

Figure 4.15: Optimisation history for Quadratic RSM saddle point Design 2

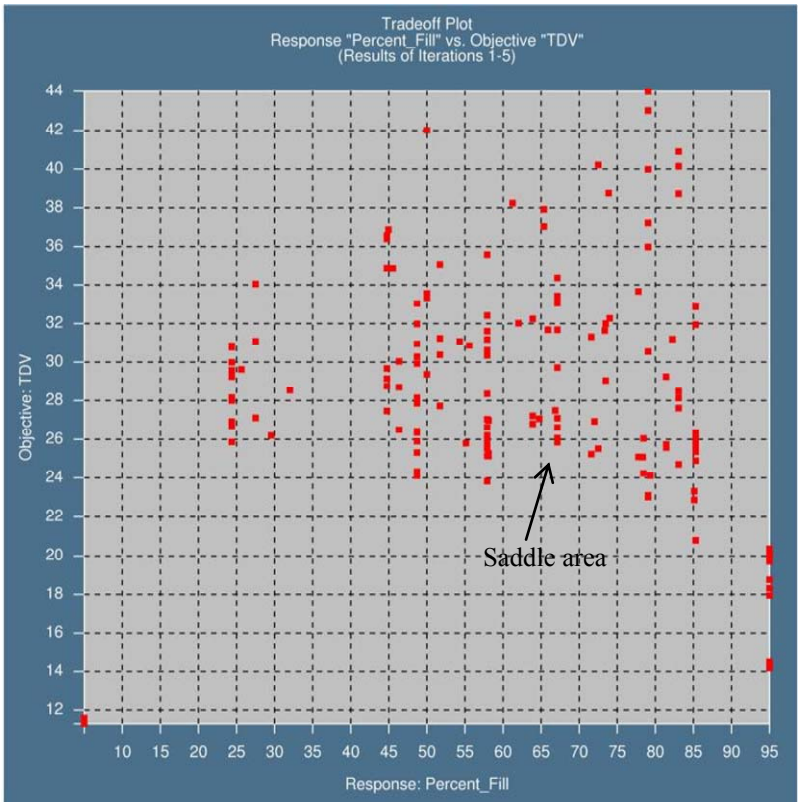

Figure 4.16: Trade-off plot for TDV versus fill level for Quadratic RSM saddle point Design 2

Figure 4.16 above shows all the analysis points plotted as TDV against Percentage fill. The trend clearly illustrates the reduction in sloshing due to extreme fill levels. The data conforms well to what is suggested in the literature, as discussed in section 2.4.2 of this dissertation. The spread of values for a given fill level represents the various designs considered for that fill level, and illustrates the variation in performance of those designs. Figure of between 69 % and 77% full for the worst case TDV in the last 3 optimisation iterations support the previous use of 70% full as a fill level. The implication is that other fill levels would exhibit less sloshing for the same set of design variable values (hence the notation of a saddle point).

4.4.2.8 Summary of 2D optimisation results

Table 4.11 below provides a summary of the 2D-sloshing optimisation results presented in this chapter.

Table 4.11: Summary of 2D-sloshing optimisation results

Case	TDV (start) $f*10^4$ [m.s]	TDV (final) $f*10^4$ [m.s]	TDV best data point $f*10^4$ [m.s] (Iteration)	Total baffle length [mm]	Design variables (Start)	Design variables (final)	Total iterations	Function Evaluations	Active constraints
1	36.46	22.66	22.66 (8.1)	373.8	(Hc,Hb,S) (100,100,50)	(Hc,Hb,S) (77.28,134.6, 10)	10	50	g_2,g_6
2	36.46	23.26	22.9 (8.3)	370.8	(Hc,Hb,S) (100,100,50)	(Hc,Hb,S) (76.68,133.6, 10)	8	128	g_2,g_6
3	36.46	26.41	22.9 (1.115)	349.5	(Hc,Hb,S) (100,100,50)	(Hc,Hb,S) (73.24,126.5, 10)	1	129	g_2,g_6
4	36.46	23.18	23.18 (10)	378	(Hc,Hb,S) (100,100,50)	(Hc,Hb,S) (78,136,10)	10	40	g_2,g_6
5	27.03	22.52	22.52 (7.1)	418.8	(MBC,SBC, MBH,SBW) (100,100, 100,100)	(MBC,SBC, MBH,SBW) (80.8,79.29, 141.6,138.6)	8	184	g_4
6	33.56	29.37	29.37 (11.1)	516	(MBC,SBC, MBH,SBW) (100,100, 100,100)	(MBC,SBC, MBH,SBW) (162,78, 244,136)	10	81	g_4
7	33.56	24.23	-	443	(F,MBC,SBC, MBH,SBW) (100,100, 100,100,0.1)	(F,MBC,SBC, MBH,SBW) (0.153,84,86, 139,152)	8	257	g_4

It is interesting to note that although most optimum values coincide with the best data point for the particular case, the two cases that do not (Case 2 and 3) use the same data set. It should be once again noted that the data points used for the nueral network are supplied by the database of points available from the quadratic SRSM (Case 2) analysis. The suspicion is that in both cases, insufficient resolution of points were

available near the optimum and that further optimisation iterations would have in all likelihood resulted in more accurate predictions of the location of the local minimum.

The Linear RSM analyses provided very similar final results to the Quadratic RSM analyses with fewer function evaluations, e.g., 50 (Case 1) and 128 (Case 2) function evaluations for the Linear and Quadratic RSMs respectively for design 1. If one is interested in the optimum result only, one would therefore favour the Linear RSMs. If however one is interested in the trends exhibited for each design problem, one requires a higher level of confidence in the quality of the fit with respect the response in question. Figure 4.17 below provides some insightful data in this respect. The bar graphs provided represent ANalysis Of VAriance (ANOVA) [34] plots for both the Linear and Quadratic RSM analyses of the design 1 liquid container. Both plots are for the 3rd optimisation iteration of their respective analyses. Each bar represents a specific term in the equation which corresponds to the response surface fitted through the data for that optimisation iteration. Intuitively, the Linear fit requires only three (the number of variables) terms, as interaction effects are not considered, while the quadratic fit requires nine terms. The magnitudes of the bars relative to each other illustrate the relative significance of that term in the fit. The magnitude of the red portion of the bar provides a relative indication of the confidence in the value of the coefficient chosen for that term.

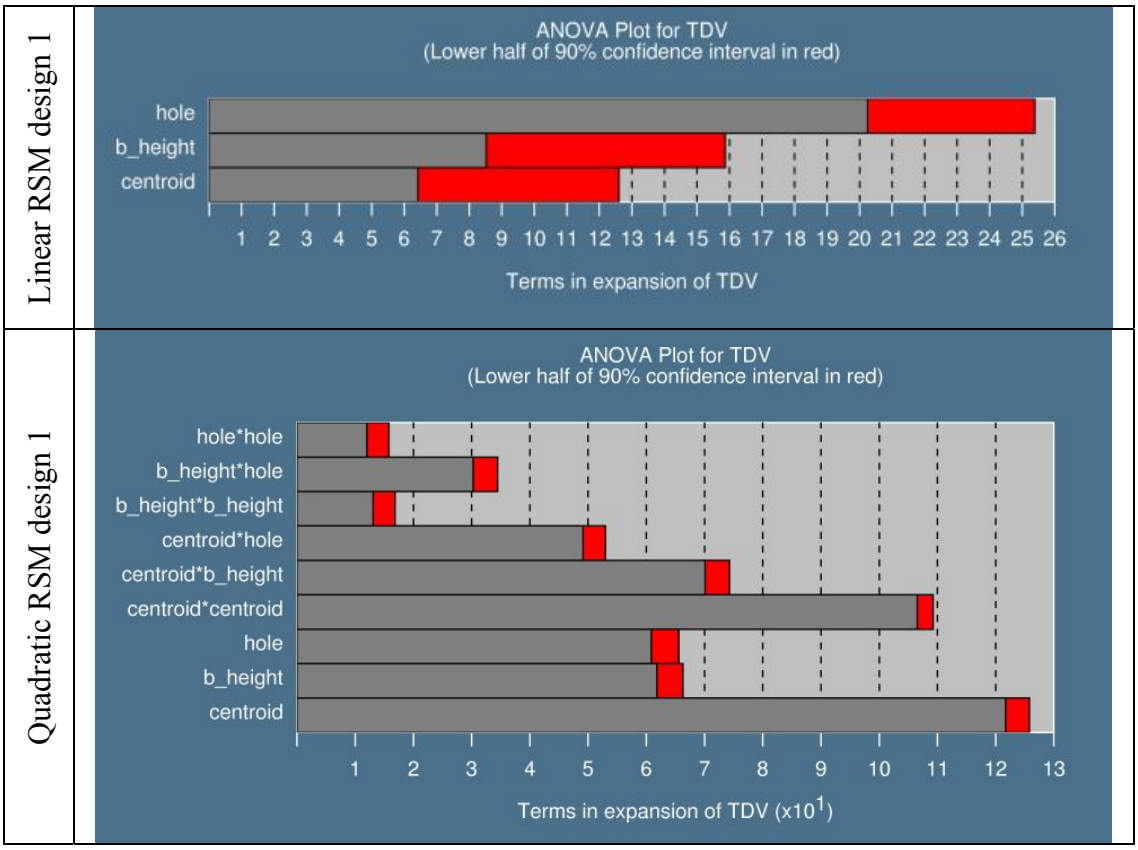

Figure 4.17: Comparative ANOVA plots for Quadratic and Linear RSM analyses

It is clear from the plots that the quadratic fit provides a surface in which the optimisation algorithm has significantly higher confidence. The plot also shows that the quadratic cross or interaction terms are as significant as the linear terms. These data provide strong motivation for the use of a Quadratic RSM if the trends in the performance of the design are of significant interest, e.g., when considering trade offs.

4.5 Conclusion

The main point that can be concluded form this chapter is that RSMs in conjunction with LS-OPT provide a robust and insightful method of numerical design optimisation of liquid containers for sloshing. The over-sampling method used by LS-OPT ensures minimal susceptibility to noise and a good estimation of the response for the specific design subspace.

A final observation from this chapter is that global meta-model methods like Kriging and Neural Networks can provide interesting plots when contemplating global trends for up to two variables.